

Near-Field Velocity Estimation and Predictive Beamforming with Modular Linear Array

Khalid A. Alshumayri, Mudassir Masood *Senior Member, IEEE*, Ali A. Nasir, *Senior Member, IEEE*

arXiv:2511.06383v1 [eess.SP] 9 Nov 2025

Abstract—Velocity estimation is a cornerstone of a recently introduced near-field predictive beamforming. This paper derives the closed-form Cramér–Rao bounds (CRBs) for joint velocity estimation using a modular linear array (MLA) within a predictive-beamforming framework. The analysis shows that increasing inter-module separation enlarges the effective aperture and reduces the transverse-velocity CRB, whereas the radial-velocity CRB is largely insensitive to separation. We further obtain a simple closed-form relation linking the achievable antenna savings to the inter-module separation while preserving the same transverse accuracy of a uniform linear array (ULA). We further investigate how velocity mismatch affects array gain and show that transverse-velocity errors cause more severe performance degradation than radial-velocity errors. Simulations show that predictive beamforming with MLAs maintains high localization accuracy for target tracking.

Index Terms—Near-field, integrated sensing and communications (ISAC), predictive beamforming, velocity estimation.

I. INTRODUCTION

The adoption of ELAs expands the near-field (NF) region, enabling estimation of radial and transverse velocities from wavefront curvature. As the aperture grows, the Fraunhofer distance expands, placing users within the NF region, where spherical wavefronts produce a nonuniform phase across the aperture. This curvature enables joint inference of range and direction of arrival (DoA) and, for moving targets, makes both radial and transverse velocity components observable via element-dependent Doppler [1]–[3]. Such capabilities are attractive for integrated sensing and communications (ISAC), e.g., cellular-connected UAVs and vehicle-to-everything networks (V2X), where predictive beamforming uses estimated velocities to compensate for Doppler and forecast user motion while reducing pilot overhead [4], [5]. Recent predictive-beamforming work proposed a maximum-likelihood estimator (MLE) for radial/transverse velocities in the NF region, but did not analyze performance bounds [3]. However, this pioneer work did not analyze the performance bound on the estimation accuracy of the proposed scheme. In contrast, [6] derived the Cramér–Rao lower bounds (CRBs) for estimating radial and transverse velocities using ULA, but their analysis was limited to a single-input multiple-output (SIMO) configuration, which differs from the predictive beamforming framework.

Realizing beamforming with a large number of antennas poses significant challenges in both hardware and signal processing. To address this, the modular linear array (MLA)

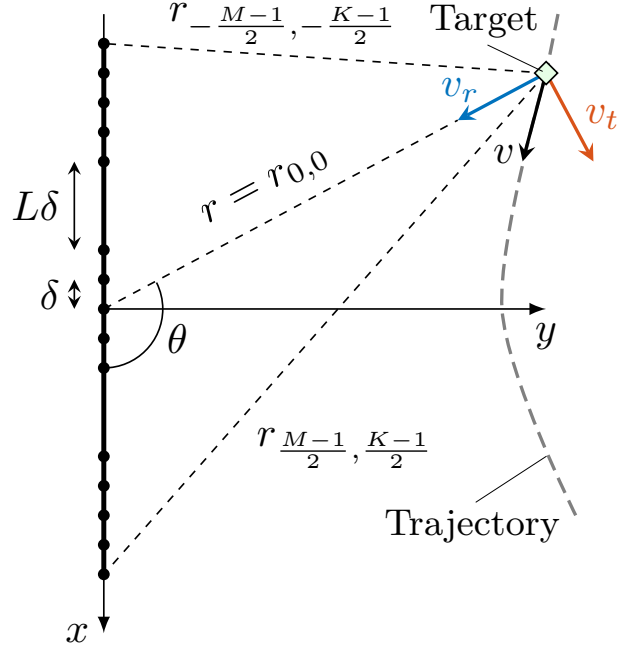


Fig. 1. Illustration of the near-field velocity sensing employing a modular array.

architecture achieves a larger aperture without adding more antennas. MLA grows the effective aperture by grouping elements into uniform linear array (ULA) modules separated by larger inter-module spacings as in Fig. 1, easing deployment on rooftops or façades while extending the NF region [7]–[10]. Prior work on MLA has derived the CRBs for range and angle estimation [11], and extends the analysis to MLA with non-uniform inter-module spacing [12].

In this paper, the CRBs for the joint estimation of radial and transverse velocities using MLA are derived. This paper makes three contributions. (i) We derive tractable, closed-form CRBs for joint radial and transverse velocity estimation with MLAs in the NF region, revealing explicit dependence on array parameters and inter-module separation. (ii) We obtain a closed-form expression for the predictive-beamforming array gain under velocity mismatch and show that transverse-velocity errors contribute more severely to signal-to-noise ratio (SNR) degradation compared to radial-velocity errors. (iii) We establish a practical design rule: enlarging inter-module separation reduces the transverse-velocity CRB via effective-aperture growth, while the radial-velocity CRB remains essentially unchanged. Simulations validate the analysis, showing

2.9 dB transverse-CRB improvement at an inter-module separation 25% of the original ULA length. In addition, with the same separation, a 198-element MLA achieves the transverse-velocity accuracy of a 240-element ULA with a modest 1.6 dB radial-CRB penalty.

II. NEAR-FIELD VELOCITY SENSING AND PREDICTIVE BEAMFORMING

A. Signal and System Model

As illustrated in Fig. 1, we consider a near-field communications system. The base station (BS) is equipped with a modular ELAA composed of K modules, each with M antennas, resulting in a total of MK antennas. The antenna spacing is uniform and denoted by δ . The modules are placed evenly along the x -axis with an inter-module spacing $L\delta$ and symmetric around the origin. The location of the m -th element in the k -th module is given by the vector $\mathbf{w}_{m,k} = [x_{m,k}, 0]^T$ where $m = 0, \pm 1, \dots, \pm \frac{M-1}{2}$, $k = 0, \pm 1, \dots, \pm \frac{K-1}{2}$. The coordinates are given by $x_{m,k} = (Uk + m)\delta$, where $U = M + L - 1$. Further, the same antenna array is employed for transmitting and receiving, made possible by circulators and full-duplex capability [13]. The (m, k) -th entry of the array response vector at time index n is given by [2], [3]

$$[\mathbf{a}_n(r, \theta, v_r, v_t)]_{m,k} = \exp \left\{ -j \frac{2\pi}{\lambda} (r_{m,k} + v_{m,k} nT_s) \right\} \quad (1)$$

where $r_{m,k} = \sqrt{r^2 - 2r(Uk + m)\delta \cos \theta + (Uk + m)^2 \delta^2}$ is the distance between the target and the m, k -th antenna of module k , T_s is the symbol duration. The Doppler shift is caused by $v_{m,k} = q_{m,k}v_r + p_{m,k}v_t$, where v_r and v_t denote the radial and transverse velocities of the target with respect to the origin, $q_{m,k}$ and $p_{m,k}$ denote the projection coefficients

$$q_{m,k} = \frac{r - (Uk + m)\delta \cos \theta}{r_{m,k}}, \quad p_{m,k} = \frac{(Uk + m)\delta \sin \theta}{r_{m,k}}, \quad (2)$$

which satisfy $q_{m,k}^2 + p_{m,k}^2 = 1$, and if the FF approximation is used such that $r_{m,k} \approx r - (Uk + m)\delta \cos \theta$, it will result in $q_{m,k} = 1$ and $p_{m,k} = 0$, which explains the reason the transverse velocity remains unobservable under that model. However, for the NF region, this approximation is no longer valid. In addition, we assume the target movement is confined within the radiating NF region, specifically at a distance greater than the Fresnel distance [14], which is defined as $d_F = 0.5\sqrt{A^3/\lambda}$ where $A = \delta[K(M-1) + L(K-1)]$ is the aperture length, which can equivalently be expressed as $A = \delta[U(K-1) + M-1]$.

For notation convenience, let ϕ represent the target parameters $\{r, \theta, v_r, v_t\}$. Assuming that the downlink channel between BS and target is dominated by the line-of-sight (LoS) component of the channel, the received baseband echo signal at the array, reflected by the moving target, at time index n for the l -th coherent processing interval (CPI) will be described as

$$\mathbf{y}_l(n) = \beta \mathbf{a}_n(\phi_l) \mathbf{a}_n^T(\phi_l) \mathbf{x}(n) + \mathbf{z}(n) \quad (3)$$

where $\beta \in \mathbb{C}$ represents the reflection coefficient that depends on both the round-trip pathloss and the radar cross section (RCS), $\mathbf{z}(n)$ is circular white Gaussian noise. The transmit signal $\mathbf{x}(n)$ is designed according to the estimated parameters ϕ from the previous CPI. This is the idea of predictive beamforming proposed in [3].

B. Predictive Beamforming

The advantages of employing predictive beamforming in designing the transmit signal $\mathbf{x}(t)$ are twofold: 1) Doppler compensation and prediction of the target's future location, and 2) eliminating the need for pilot symbols, or prior knowledge of the target motion by utilizing the kinematic model

$$\hat{r}_{l+1} = \hat{r}_l + \hat{v}_{r,l} NT_s, \quad \hat{\theta}_{l+1} = \hat{\theta}_l + \hat{v}_{t,l} NT_s / \hat{r}_l. \quad (4)$$

The predicted parameters ϕ are used to steer the beam in the next CPI. Accordingly, the transmit signal is designed as

$$\mathbf{x}(n) = \frac{\mathbf{a}_n^*(\hat{\phi}_l)}{\sqrt{MK}} s_n \quad (5)$$

where s_n represents the information symbol that satisfy $|s_n|^2 = 1$. A rough estimate of the parameters v_r and v_t can be obtained from the previous CPI and used in the current CPI to compensate for the Doppler shift and predict the target's future location. Substituting (5) into (3), the received echo signal at the BS will be ¹

$$\mathbf{y}_l(n) = \beta \psi(n) \mathbf{a}_n(\phi_l) s_n + \mathbf{z}(n) \quad (6)$$

where $\psi(n)$ is the array gain under velocity mismatch

$$\psi(n) = \frac{1}{\sqrt{MK}} \sum_{m,k} e^{-j \frac{2\pi}{\lambda} (q_{m,k} \Delta v_r + p_{m,k} \Delta v_t) n T_s} \quad (7)$$

Here, Δv_r and Δv_t denote the mismatches between the true and estimated radial and transverse velocities, respectively. To simplify $\psi(n)$, we adopt the approximation introduced in [15], under which $q_{m,k} \approx 1$ and $p_{m,k} \approx \frac{(Uk+m)\delta \sin \theta}{r}$.

$$\psi(n) \approx \frac{e^{-j \frac{2\pi}{\lambda} \Delta v_r n T_s}}{\sqrt{MK}} \left(\sum_m e^{-j \alpha m} \right) \left(\sum_k e^{-j \alpha U k} \right), \quad (8)$$

where $\alpha = \frac{2\pi}{\lambda} \left(\frac{\delta \sin \theta}{r} \right) \Delta v_t n T_s$. The summation can be recognized as a Dirichlet kernel-type finite geometric sum. Hence, the closed-form expression of $\psi(n)$ is given by

$$\psi(n) = \frac{e^{-j \frac{2\pi}{\lambda} \Delta v_r n T_s}}{\sqrt{MK}} \frac{\sin(M\alpha/2)}{\sin(\alpha/2)} \frac{\sin(KU\alpha/2)}{\sin(U\alpha/2)}. \quad (9)$$

Ideally, when $\hat{v}_r \approx v_r$ and $\hat{v}_t \approx v_t$, the array gain satisfies $\psi(n) \approx \sqrt{MK}$, which is numerically demonstrated in Section IV. Therefore, noise-free version of the received signal at the BS is given by

$$\mu_n = \beta \sqrt{MK} \mathbf{a}_n(\phi) s_n. \quad (10)$$

¹A similar derivation would apply for the uplink scenario if the signal is known (i.e., pilot signal), then $\mathbf{y}_l(n) = \beta \mathbf{a}_n(\phi_l) s_n$

Moreover, applying the point scatter model, the reflection coefficient can be expressed as [16]

$$|\beta|^2 = \frac{G_t G_r \lambda^2 \sigma_{RCS}}{(4\pi)^3 r^4}, \quad (11)$$

where σ_{RCS} represents the radar cross-section, while, G_t and G_r denote the antenna gains for transmitter and receiver respectively. For a monostatic setup, the antenna gains are equal, i.e., $G_r = G_t$.

III. VELOCITY & LOCATION ESTIMATION

The CRB provides a theoretical lower limit on the variance of unbiased estimators of a deterministic parameter. It is derived from the Fisher Information, which quantifies the amount of information that an observable random variable carries about an unknown parameter. The Fisher information matrix (FIM) for radial and transverse velocity is given by

$$\mathbf{F} = \begin{bmatrix} J_{v_r v_r} & J_{v_r v_t} \\ J_{v_t v_r} & J_{v_t v_t} \end{bmatrix}.$$

Let the unknown parameters $\zeta = [v_r \ v_t]^T$, the FIM elements under the white Gaussian noise model can be found as

$$J_{ij} = \frac{2}{\sigma^2} \sum_n \sum_m \sum_k \Re \left\{ \frac{\partial \boldsymbol{\mu}_n^H}{\partial \zeta_i} \frac{\partial \boldsymbol{\mu}_n}{\partial \zeta_j} \right\}.$$

Accordingly, the three FIM elements can be readily obtained

$$J_{v_r v_r} = \gamma MK \sum_{m,k} q_{m,k}^2, \quad (12)$$

$$J_{v_t v_t} = \gamma MK \sum_{m,k} p_{m,k}^2, \quad (13)$$

$$J_{v_r v_t} = \gamma MK \sum_{m,k} q_{m,k} p_{m,k}, \quad (14)$$

where γ is given by

$$\gamma = \left(\frac{2\pi}{\lambda} \right)^2 \frac{|\beta|^2 N(N+1)(2N+1)}{3\sigma^2} T_s^2,$$

The CRBs for radial and transverse velocities correspond to the diagonal elements of the inverse of the FIM.

$$\text{CRB}(v_r) = \frac{J_{v_t v_t}}{\text{Det } \mathbf{F}}, \quad \text{CRB}(v_t) = \frac{J_{v_r v_r}}{\text{Det } \mathbf{F}}. \quad (15)$$

To obtain more tractable CRB expressions, we employ a simple yet tight approximation. In particular, the expressions in (13) and (14) can be simplified using the following lemma.

Lemma 1: Consider a target located at a distance $r \geq d_F$, and assume that the aperture length satisfies $U(K-1) + M - 1 \gg \lambda/\delta$. Then, the following approximation holds:

$$\sum_{m,k} p_{m,k}^2 = \frac{MK}{12} \left(U^2(K^2-1) + (M^2-1) \right) \frac{\delta^2}{r^2} \sin^2 \theta, \quad (16)$$

$$\sum_m q_{m,k} p_{m,k} = \frac{MK}{12} \cdot \left(U^2(K^2-1) + (M^2-1) \right) \frac{\delta^2}{r^2} \cos \theta \sin \theta. \quad (17)$$

Proof: Please refer to Appendix A ■

For a standard uniform linear array, $\lambda/\delta = 2$, hence the condition $U(K-1) + M - 1 \gg 2$ is typically satisfied. The expression (16) show that the information on transverse velocity increases with inter-module separation due to the larger effective aperture size. Moreover, we can derive the closed-form CRBs as in the following theorem.

Theorem 1: For a target located at a distance $r \geq d_F$ and for $M-1 \gg \lambda/\delta$, the CRBs for radial and transverse velocities are given by

$$\text{CRB}_{\text{Mod}}^{(v_r)} = \left(\frac{\lambda}{2\pi} \right)^2 \frac{12}{\gamma(MK)^2 \left(12 - \left(\frac{\delta}{r} \right)^2 (U^2(K^2-1) + M^2-1) \right)}, \quad (18)$$

$$\text{CRB}_{\text{Mod}}^{(v_t)} = \left(\frac{\lambda}{2\pi} \right)^2 \frac{r^2}{\gamma(MK)^2 \delta^2 (U^2(K^2-1) + M^2-1) \sin^2 \theta}. \quad (19)$$

Proof: Please refer to Appendix B ■

Note that the radial CRB is not a function of the target angle. Increasing the inter-module spacing reduces the transverse-CRB while the radial-CRB is less affected due to the small term $(\delta/r)^2$. Additionally, for the special case when $L = 1$ and $M_o = MK$, the result is reduced to the CRB for the conventional ULA in [6]

$$\text{CRB}_{\text{ULA}}^{(v_r)} = \left(\frac{\lambda}{2\pi} \right)^2 \frac{12}{\gamma M_o^2 \left(12 - \left(\frac{\delta}{r} \right)^2 (M_o^2-1) \right)}, \quad (20)$$

$$\text{CRB}_{\text{ULA}}^{(v_t)} = \left(\frac{\lambda}{2\pi} \right)^2 \frac{r^2}{\gamma M_o^2 \delta^2 (M_o^2-1) \sin^2 \theta}. \quad (21)$$

Because $\delta/r \ll 1$, the radial CRBs are much smaller than their transverse counterparts, as verified numerically in Section IV. Since increased inter-module spacing can yield $\text{CRB}_{\text{Mod}}^{(v_t)} < \text{CRB}_{\text{ULA}}^{(v_t)}$, it is natural to ask whether we can trade antennas for aperture by widening the spacing while reducing the number of elements, so that the modular array CRB matches the ULA CRB. Formally, we seek parameters for which

$$\text{CRB}_{\text{ULA}}^{(v_t)} = \text{CRB}_{\text{Mod}}^{(v_t)}. \quad (22)$$

Concretely, for some choice of inter-module separation L and per-module size \bar{M} satisfying $K\bar{M} < M_o$, the modular array's CRB equals that of the ULA. For that purpose, the inter-module spacing is written in units of the reference ULA aperture, $L = 1 + \eta(M_o - 1)$, where η denotes the fraction of the ULA aperture added as extra spacing between adjacent modules, and the case $\eta = 0$ reduces to the standard ULA configuration. The minimum separation that achieves the same performance as ULA is given by

$$\eta = \frac{1}{M_o - 1} \left(\sqrt{\frac{M_o^2(M_o^2-1) - (\bar{M}^2-1)(\bar{M}K)^2}{(K^2-1)(\bar{M}K)^2}} - \bar{M} \right). \quad (23)$$

To determine the amount of antenna saved (i.e., $K\bar{M}/M_o$), we resort to the approximation in the following proposition.

Proposition 1: Let $K \in \mathbb{N}$ and $K \geq 1$, and let M_o be sufficiently large. Then, for η in a neighborhood of zero, the normalized array size $\frac{K\bar{M}}{M_o}$ admits the second-order expansion,

$$\frac{K\bar{M}}{M_o} = 1 - \frac{K^2 - 1}{2K} \eta + \frac{(K^2 - 1)(K^2 - 3)}{8K^2} \eta^2 + \mathcal{O}(\eta^3). \quad (24)$$

Proof: Please see Appendix C. \blacksquare

Equation (24) characterizes the antenna savings as a function of the number of modules K and the inter-module separation η . Equivalently, the fraction of antennas saved is $1 - K\bar{M}/M_o$. In the limiting cases $\eta = 0$ (no inter-module spacing) or $K = 1$ (a single module), the MLA reduces to a ULA, and $K\bar{M}/M_o = 1$.

IV. NUMERICAL RESULTS

This section presents numerical results that validate the derived CRB expressions for a modular linear array. The carrier frequency is fixed at 28 GHz, while the system bandwidth and the CPI are set to $B = 100$ kHz and 2 ms, respectively. This corresponds to a pulse width of $T_s = 10^{-5}$ s and a total of $N = 200$ symbols per CPI.

Fig. 2 shows the array-gain loss due to velocity estimation errors. Specifically, the minimum value of $|\psi(n)|^2$ within a CPI is plotted against radial and transverse velocity errors. Array-gain loss is far more sensitive to v_t mismatch than to v_r , underscoring the critical role of Doppler compensation in NF communications. Furthermore, the closed-form array gain expression in (8) is shown to match perfectly with the summation-based expression in (7).

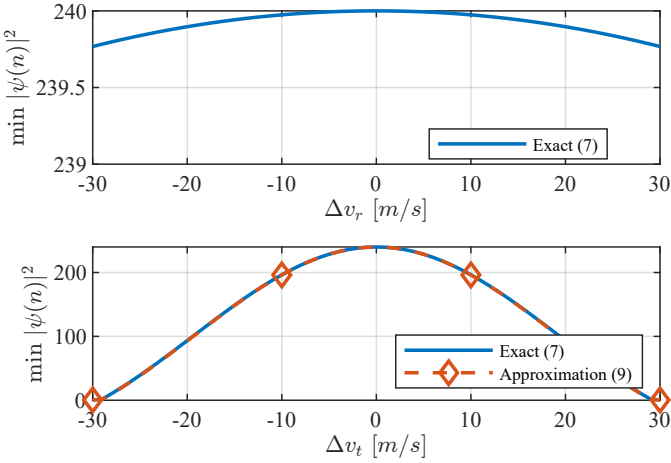


Fig. 2. Effect of velocity mismatch on the array gain when $r = d_F$, $\theta = \pi/2$.

Fig. 3 compares the derived CRBs for the MLA with those of a conventional ULA as a function of distance. For a fair comparison, the MLA aperture length is fixed at 1.6 m. The upper subfigure shows the radial-velocity CRB, which varies only mildly with distance, whereas the lower subfigure shows the transverse-velocity CRB, which increases approximately quadratically with the BS-user distance. Besides, the transverse CRB is approximately 2.9 dB improved for $K = 2$ and

$L = 61$, corresponding to an inter-module separation of 33 cm or $\eta = 0.25$. Overall, the radial-CRB is much greater than the transverse-CRB.

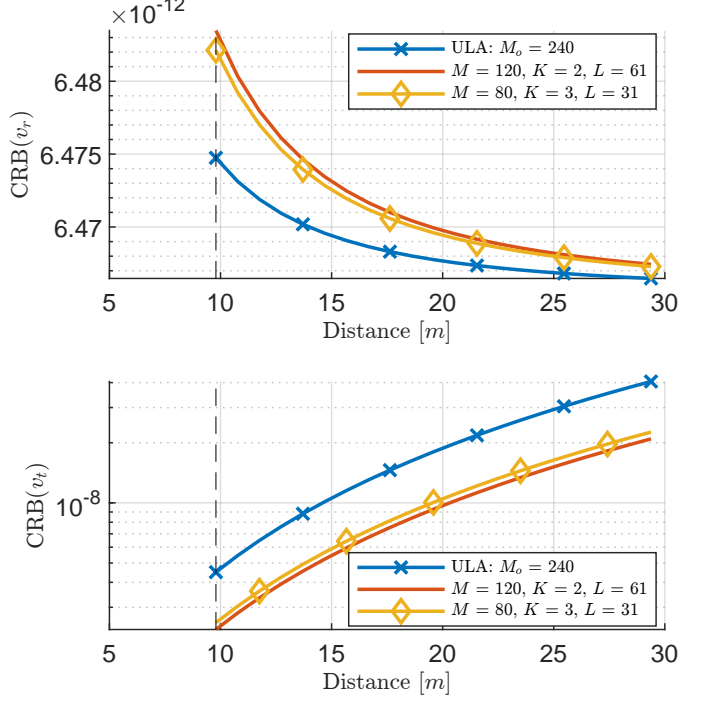


Fig. 3. CRBs versus distance for the MLA and ULA. Top: radial-velocity; bottom: transverse-velocity.

Fig. 4 revisits the ULA and the MLA (with $K = 2$ and $L = 61$) from Fig. 3 and adds two 198-element MLAs. The first 198-element design (solid, $L = 61$, $K = 2$, and $\bar{M} = 99$) matches the 240-element ULA's transverse-velocity CRB while using about 17% fewer elements. The trade-off is about 1.6 dB increase in radial-velocity CRB. The second 198-element design (dashed, $L = 103$, $K = 2$, and $\bar{M} = 99$) attains the same aperture as the 240-element MLA and further improves the transverse-velocity CRB, with essentially the same radial-velocity behavior. These comparisons confirm that enlarging inter-module separation reduces the transverse-velocity CRB through effective-aperture growth, whereas the radial-velocity CRB is largely insensitive to separation because the dependence enters only via the small squared ratio $(\delta/r)^2$ in (18).

Fig. 5 plots the inter-module separation factor η against the number of antennas required to match the ULA performance. The *Exact* curves are obtained from the analytic expression (23) and the *Approximation* curves follow the second-order series (24). The second-order approximation matches the exact result for small η and diverges as η increases. Additionally, increasing K expands the array aperture, further reducing the required antenna count.

The performance of the predictive-beamforming scheme is shown in Fig. 6. The trajectory is predicted by recursively applying the kinematic update in (4) for every CPI. Tracking is initialized at $(r_0, \theta_0) = (d_F, \pi/4)$ and runs for 300 CPIs. In addition, we set $G_t = G_r = 1$ and $\sigma_{RCS} = -23$ dB. The noise

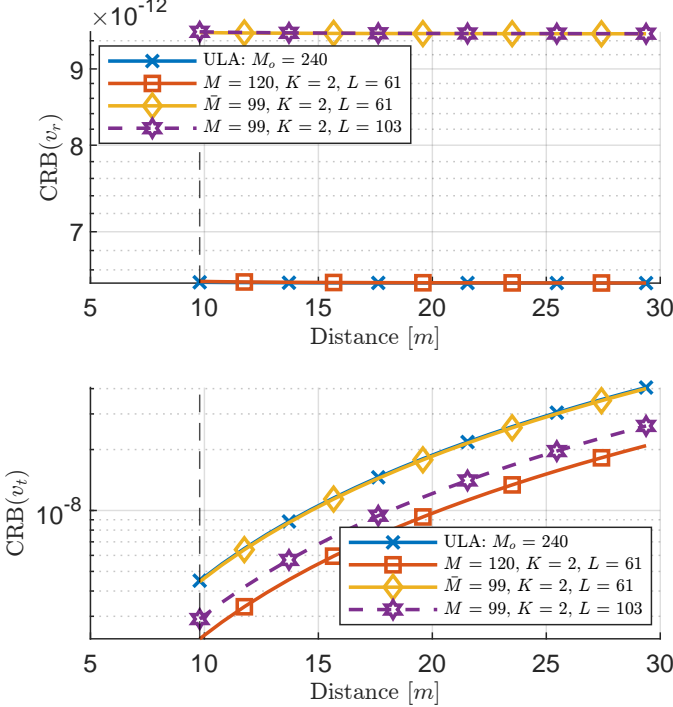


Fig. 4. CRB for radial velocity (top) and transverse velocity (bottom), with $\theta = \pi/2$. The gray dashed line represents the Fresnel distance.

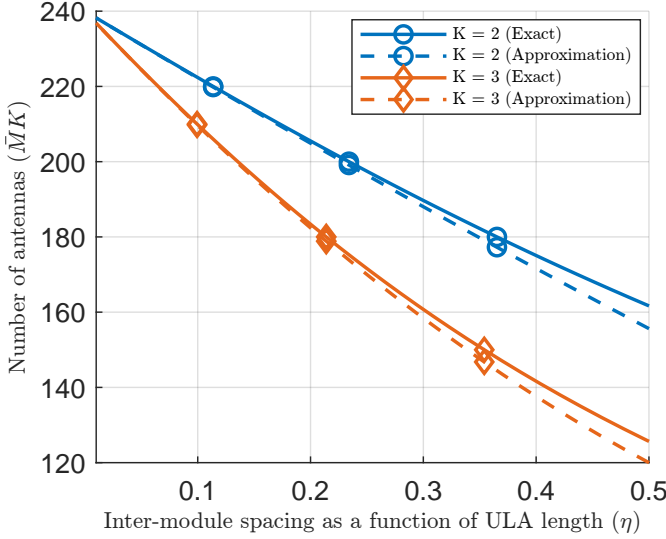


Fig. 5. The separation between modules η versus the number of antennas MK , required to achieve ULA-level CRB with 240 antennas.

density power is set to -174 dBm/Hz. In this experiment, the true velocities are $v_r = 10$ m/s and $v_t = 8$ m/s.

V. CONCLUSION

In this paper, the CRBs for joint radial- and transverse-velocity estimation with MLAs in the near field are derived. In addition, we establish a closed-form characterization of array gain under velocity mismatch, revealing that inaccurate transverse-velocity compensation results in degraded beamforming gain. Further, we obtain a closed-form relation linking

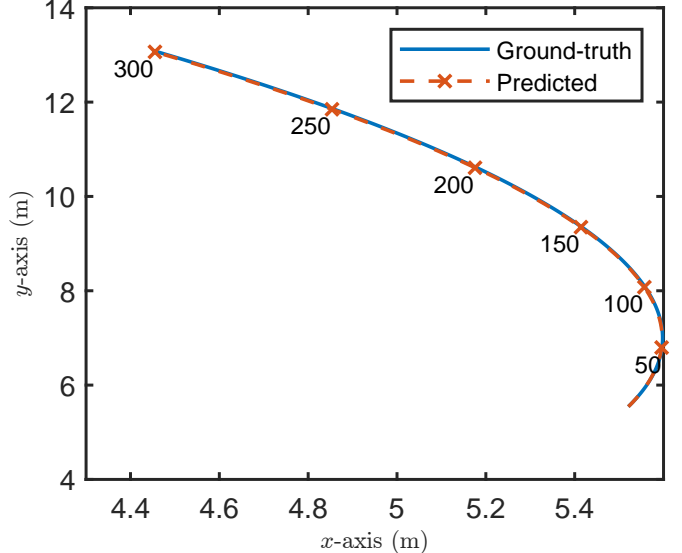


Fig. 6. Predicted trajectory of the moving target. Labels are shown every 50 CPIs.

the fraction of antennas saved to the chosen inter-module separation, while preserving the same transverse accuracy of ULA. Our results also show that increasing inter-module separation enlarges the effective aperture and reduces the transverse-velocity CRB, whereas the radial-velocity CRB is largely insensitive to separation. Simulation results show that, with intermodule separation equal to 25% of the reference ULA length, a 198-element MLA attains the transverse-velocity CRB of a 240-element ULA, saving 17% of antennas, at a cost of only 1.6 dB in radial-velocity accuracy due to the reduction in antenna number. These results demonstrate that MLAs can deliver ULA-level near-field sensing with fewer antennas.

APPENDIX A PROOF OF LEMMA 1

To simplify the summation in (13), set $g = U\kappa + m$ and $\epsilon = \delta/r$,

$$p_{m,k}^2 = \frac{(g\epsilon \sin \theta)^2}{1 - 2(g\epsilon) \cos \theta + (g\epsilon)^2}, \quad (25)$$

Let $x = g\epsilon$ and define the function $f(x) \triangleq \frac{x^2 \sin^2 \theta}{1 - 2x \cos \theta + x^2}$ and observe that, $x \in [-x_0, x_0]$, where the maximum value of x occurs at the edge of the array i.e., $x_0 = (U \frac{K-1}{2} + \frac{M-1}{2}) \epsilon$. Given that $\epsilon \ll 1$ and its maximum value occurs at the Fresnel distance when $\epsilon = \delta/d_F$, then

$$\max\{|x_0|\} = \sqrt{\frac{\lambda/\delta}{U(K-1) + (M-1)}}, \quad (26)$$

The term $|x_0|$ can be made arbitrary small if and only if $U(K-1) + M-1 \gg \lambda/\delta$. Then using Taylor series expansion around $x = 0$, we can write $f(x) \approx x^2 \sin^2 \theta$ and since $p_{m,k}^2 = f(g\epsilon) \approx (\epsilon \sin \theta)^2 g^2$, then the summation becomes

$$\begin{aligned}
\sum_{m,k} p_{m,k}^2 &\approx (\epsilon \sin \theta)^2 \sum_{m,k} (Uk + m)^2, \\
&= (\epsilon \sin \theta)^2 \sum_k \sum_m (U^2 k^2 + 2Ukm + m^2), \\
&= \frac{MK}{12} (U^2(K^2 - 1) + (M^2 - 1)) \epsilon^2 \sin^2 \theta.
\end{aligned} \tag{27}$$

Similarly, using Taylor expansion, one can approximate the off-diagonal term (14) as

$$\begin{aligned}
q_m p_m &= \frac{g\epsilon \sin \theta (1 - g\epsilon \cos \theta)}{1 - 2(g\epsilon) \cos \theta + (g\epsilon)^2}, \\
&\approx g\epsilon + (g\epsilon)^2 \sin \theta \cos \theta,
\end{aligned}$$

Note that, due to symmetry, $\sum_{m,k} g = \sum_{m,k} Uk + m = 0$, hence the summation becomes

$$\sum_m q_m p_m \approx \frac{MK}{12} (U^2(K^2 - 1) + M^2 - 1) \epsilon^2 \sin \theta \cos \theta, \tag{28}$$

Therefore, the proof of Lemma 1 is completed.

APPENDIX B PROOF OF THEOREM 1

Using the derived expressions (27) and (28) in Lemma 1, the determinant of the FIM \mathbf{F} is given by

$$\begin{aligned}
\det(\mathbf{F}) &= J_{v_r v_r} J_{v_t v_t} - J_{v_r v_t}^2, \\
&= \gamma^2 (MK)^2 \left[\left(\sum_m q_m^2 \right) \left(\sum_m p_m^2 \right) - \left(\sum_m q_m p_m \right)^2 \right], \\
&\approx \gamma^2 (MK)^2 \sin^2 \theta [MK - G\epsilon^2] G\epsilon^2,
\end{aligned} \tag{29}$$

where $G = MK (U^2(K^2 - 1) + M^2 - 1) / 12$. The existence of the CRB is guaranteed when $\frac{12}{U^2(K^2-1)+M^2-1} > \epsilon^2$, which holds for $r \geq d_F$ and $U(K - 1) + M - 1 \gg \lambda/\delta$. Therefore, the approximate CRBs for the radial and transverse velocities are given by

$$\text{CRB}(v_r) \approx \frac{1}{\gamma(MK)^2 (MK - G\epsilon^2)}, \tag{30}$$

$$\text{CRB}(v_t) \approx \frac{12}{\gamma(MK)^2 G\epsilon^2 \sin^2 \theta} \underbrace{\left(\frac{MK - G\epsilon^2 \sin^2 \theta}{MK - G\epsilon^2} \right)}_{\approx 1}. \tag{31}$$

where the underbraced term is a factor that is close to unity for large MK and small ϵ . Thus, the proof of Theorem 1 is completed.

APPENDIX C PROOF OF PROPOSITION 1

Let $h \triangleq \bar{M}K/M_o$. Then (23) can be rewritten as

$$h^2(K^2 - 1) \left(\frac{h}{K} + \eta \left(1 - \frac{1}{M_o} \right) \right)^2 = 1 - \frac{1}{M_o} - h^2 \left(\frac{h^2}{K^2} - \frac{1}{M_o} \right).$$

For $M_o \gg 1$ (neglecting terms of order M_o^{-1}), (32) reduces to

$$F(h, \eta) \triangleq h^4 + \frac{2(K^2 - 1)}{K} h^3 \eta + (K^2 - 1) h^2 \eta^2 - 1 = 0. \tag{32}$$

Since $F(1, 0) = 0$ and

$$\frac{\partial F}{\partial h}(h, \eta) = 4h^3 + \frac{6(K^2 - 1)}{K} h^2 \eta + 2(K^2 - 1)h \eta^2,$$

we have $\frac{\partial F}{\partial h}(1, 0) = 4 \neq 0$. By the implicit function theorem, there exists a unique differentiable function $u(\eta)$ in a neighborhood of $\eta = 0$ such that $u(0) = 1$ and $F(u(\eta), \eta) = 0$. Expanding $u(\eta)$ in a Taylor series about $\eta = 0$ yields

$$u(\eta) = u(0) + u'(0)\eta + \frac{1}{2}u''(0)\eta^2 + \mathcal{O}(\eta^3). \tag{33}$$

Implicit differentiation of $F(u(\eta), \eta) \equiv 0$ gives

$$u'(0) = -\frac{F_\eta(1, 0)}{F_h(1, 0)} = -\frac{K^2 - 1}{2K},$$

and a second differentiation yields

$$u''(0) = \frac{(K^2 - 1)(K^2 - 3)}{4K^2}.$$

Substituting into (33) gives

$$u(\eta) = 1 - \frac{K^2 - 1}{2K} \eta + \frac{(K^2 - 1)(K^2 - 3)}{8K^2} \eta^2 + \mathcal{O}(\eta^3). \tag{34}$$

as claimed.

REFERENCES

- [1] H. Wang, Z. Xiao, and Y. Zeng, "Cramér–rao bounds for near-field sensing with extremely large-scale mimo," *IEEE Transactions on Signal Processing*, vol. 72, pp. 701–717, 2024.
- [2] Z. Wang, P. Ramezani, Y. Liu, and E. Björnson, "Near-field localization and sensing with large-aperture arrays: From signal modeling to processing," *IEEE Signal Processing Magazine*, vol. 42, no. 1, pp. 74–87, 2025.
- [3] Z. Wang, X. Mu, and Y. Liu, "Near-field velocity sensing and predictive beamforming," *IEEE Transactions on Vehicular Technology*, 2024.
- [4] Y. Zeng, J. Lyu, and R. Zhang, "Cellular-connected uav: Potential, challenges, and promising technologies," *IEEE Wireless Communications*, vol. 26, no. 1, pp. 120–127, 2019.
- [5] M. H. C. García, A. Molina-Galan, M. Boban, J. Gozalvez, B. Coll-Perales, T. Şahin, and A. Kousaridas, "A tutorial on 5g nr v2x communications," *IEEE Communications Surveys & Tutorials*, vol. 23, no. 3, pp. 1972–2026, 2021.
- [6] C. Giovannetti, N. Decarli, and D. Dardari, "Performance bounds for velocity estimation with extremely large aperture arrays," *IEEE Wireless Communications Letters*, vol. 13, no. 12, pp. 3513–3517, 2024.
- [7] A. Kosasih, Ö. T. Demir, and E. Björnson, "Achieving beamfocusing via two separated uniform linear arrays," in *2024 58th Asilomar Conference on Signals, Systems, and Computers*, 2024, pp. 168–172.
- [8] W.-C. Kao, J.-Y. Wu, S.-H. Tsai, and T.-Y. Wang, "Fast ambiguity-free subspace-based multiple aoa estimation for hybrid linear arrays," in *2023 IEEE 34th Annual International Symposium on Personal, Indoor and Mobile Radio Communications (PIMRC)*, 2023, pp. 1–5.
- [9] X. Li, Z. Dong, Y. Zeng, S. Jin, and R. Zhang, "Multi-user modular xl-mimo communications: Near-field beam focusing pattern and user grouping," *IEEE Transactions on Wireless Communications*, vol. 23, no. 10, pp. 13 766–13 781, 2024.

- [10] X. Li, H. Lu, Y. Zeng, S. Jin, and R. Zhang, "Near-field modeling and performance analysis of modular extremely large-scale array communications," *IEEE Communications Letters*, vol. 26, no. 7, pp. 1529–1533, 2022.
- [11] S. Yang, X. Chen, Y. Xiu, W. Lyu, Z. Zhang, and C. Yuen, "Performance bounds for near-field localization with widely-spaced multi-subarray mmwave/thz mimo," *IEEE Transactions on Wireless Communications*, vol. 23, no. 9, pp. 10757–10772, Sep. 2024.
- [12] C. Meng, D. Ma, X. Chen, Z. Feng, and Y. Liu, "Cramér–rao bounds for near-field sensing: A generic modular architecture," *IEEE Wireless Communications Letters*, vol. 13, no. 8, pp. 2205–2209, 2024.
- [13] A. Sabharwal, P. Schniter, D. Guo, D. W. Bliss, S. Rangarajan, and R. Wichman, "In-band full-duplex wireless: Challenges and opportunities," *IEEE Journal on Selected Areas in Communications*, vol. 32, no. 9, pp. 1637–1652, 2014.
- [14] Y. Liu, Z. Wang, J. Xu, C. Ouyang, X. Mu, and R. Schober, "Near-field communications: A tutorial review," *IEEE Open Journal of the Communications Society*, 2023.
- [15] A. Hussain, A. Abdallah, A. Celik, and A. M. Eltawil, "Joint motion, angle, and range estimation in near-field under array calibration imperfections," *arXiv preprint arXiv:2507.13463*, 2025.
- [16] K. M. Braun, "Ofdm radar algorithms in mobile communication networks," Ph.D. dissertation, Karlsruhe, Karlsruher Institut für Technologie (KIT), Diss., 2014, 2014.